Autoresonant ion cyclotron isotope separation

J.-M. Rax[a] and J. Robiche
Laboratoire de Physique et Technologie des Plasmas, Ecole Polytechnique, 91128, Palaiseau, France

N. J. Fisch[b]
Princeton Plasma Physics Laboratory, Department of Astrophysical Sciences, Princeton University, P.O. Box 451, Princeton, New Jersey 08540

(Received 18 January 2007; accepted 28 February 2007; published online 16 April 2007)

A new isotope separation process based on selective cyclotron resonant interaction between ions and a tapered helicoidal magnetic structure is identified, analyzed, and evaluated. On the basis of a Hamiltonian analysis, the existence of a class of tapered magnetic modulation that provide a full conversion of linear momentum into angular momentum is discovered. The characteristics and parameters of this field configuration are analyzed and described. The dynamic of the nonresonant isotope is investigated in order to set up a separation criterion. This autoresonant ion cyclotron isotope separation mechanism provides an efficient alternative to other niches of enrichment process. © *2007 American Institute of Physics*. [DOI: 10.1063/1.2717882]

I. INTRODUCTION

Isotope separation, the process of concentrating specific isotopes of a chemical element, relies on various techniques. On the industrial scale, for uranium enrichment, for example, standards techniques require an enormous amount of energy and many cascade stages, making these processes costly; however, they are able to enrich a large amount of matter. On the other hand, to produce small quantities of pure isotopes, electromagnetic devices such as a Calutron and plasma separation process using *ion cyclotron resonance (ICR) heating*[1–10] are preferred but they do suffer of a very low throughout.

Therefore, the search for new effective isotope separation process able to cover a large range of chemical elements remains a goal of active research. To date, processes based on selective ion cyclotron resonance have been used for the isotope separation of various metallic elements.

In this paper, we present a new selective magnetic isotope separation process based on the ICR interaction of a monoenergetic multi-isotope ion beam with a *tapered* helicoidal magnetic structure. In a tapered undulator, the modulation of the magnetic field, i.e., the pitch of the helicoidal field lines, varies along the axial direction. As we will show below, we proved the existence of a tapered undulator providing *mass-dependent* phase-matched energy conversion from linear to angular momentum. Consequently, it provides a way to force different isotopes to follow different paths in the magnetic structure. This new isotope separation process is a mix of methods related to Calutron and ICR heating: we used a cyclotron resonance, but in a purely static field, no wave injection is needed.

To understand the advantage of a tapered helicoidal magnetic structure, let us consider a simple helicoidal magnetic field. Such a magnetic field is the sum of a homogeneous longitudinal component $\mathbf{B}_o = B_o \mathbf{e}_z$ plus a transverse rotating component $\mathbf{B}_\omega = B_\omega[\cos(kz)\mathbf{e}_x + \sin(kz)\mathbf{e}_y]$, where k is related to the undulator period λ through $k = 2\pi/\lambda$ and $(\mathbf{e}_x, \mathbf{e}_y, \mathbf{e}_z)$ is a Cartesian basis. In the reference frame of an ion entering this structure along $\mathbf{e}_z$ with velocity v_o, this ion experiences an interaction with a circularly polarized electromagnetic wave and a resonant interaction takes place between the cyclotron motion and this wave if the following resonant condition is fulfilled:

$$\omega_c = k v_o, \tag{1}$$

where $\omega_c = eB_o/m_i$ is the ion cyclotron frequency with respect to the longitudinal field, e is the ion charge, and m_i the resonant ion mass.

At resonance, the ion Larmor radius increases, i.e., ion perpendicular energy increases at the expense of its longitudinal energy (v_z decreases), so that the resonant condition Eq. (1) is no longer fulfilled. However, if the helicity k decreases in order to compensate this resonance mismatch such that

$$\omega_c = k(z) v_z(z) = k(0) v_o, \tag{2}$$

then the resonant interaction will last as long as the particle stays in the magnetic structure. This type of autoresonant dynamic provides two opportunities to perform isotope separation. First, the cyclotron frequency is different, so that resonance [Eq. (1)] takes place for one specific specie. Second, the tapering of the structure [Eq. (2)] is also mass dependent. As $k(z)$ is computed for one specific value of v_o, two different isotopes with the same kinetic energy, but different masses, will enter the undulator with different initial velocity v_o and as a result will follow different trajectories: The resonant isotope will undergo an energy exchange from the longitudinal degree of freedom towards the transverse degree of freedom, while the nonresonant isotope will suffer a weak adiabatic interaction and will propagate through the structure without a significant Larmor radius increase. Anticipating our major results, the position-dependent helicity $k(z)$ providing full autoresonant conversion from linear trans-

[a]Electronic address: rax@lptp.polytechnique.fr
[b]Electronic address: fisch@princeton.edu

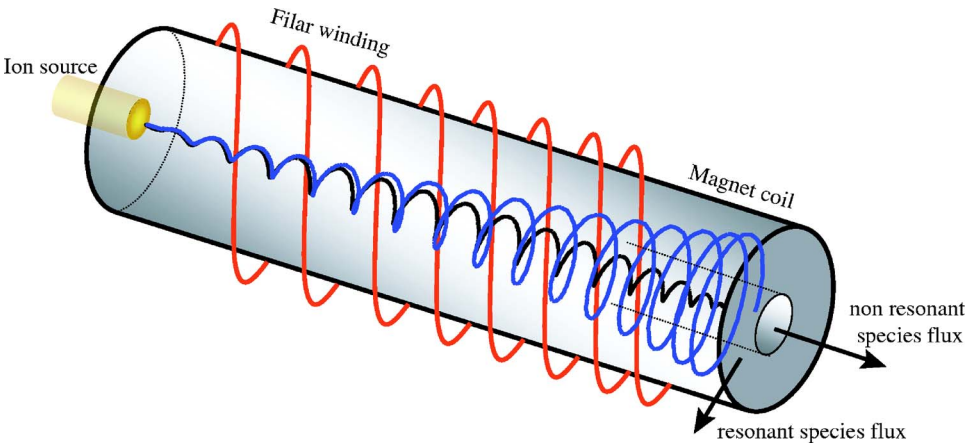

FIG. 1. Schematic of an autoresonant ion cyclotron isotope separation system.

lation to cyclotron rotation is given by the following formula:

$$k(z) = \frac{\frac{\omega_c}{v_o}}{\cos\left[2\frac{eA}{p_o}\frac{\omega_c}{v_o}z + \sum_{n=1}^{+\infty}\frac{J_n(n)}{n}\sin 2n\left(2\frac{eA}{p_o}\frac{\omega_c}{v_o}z - \frac{\pi}{2}\right)\right]}, \quad (3)$$

where J_n are Bessel functions of the first kind, A is the amplitude of the vector potential describing the rotating component of the magnetic field, and $p_o = m_i v_o$. In such a tapered magnetic undulator, one specie will arrive at the end of the structure with a large Larmor radius and the other will escape the device with a large linear momentum along the main field axis. The ultimate collection of the material on receiver or on collector plates achieves the full separation process; the issues associated with this collection process are not addressed in this paper. This process is a deterministic process and the isotopes of the chemical elements are physically separated after a single pass through the magnetic structure, as opposed to statistical processes requiring cascading. Moreover, it can be applied, as we will see later, to any elements, making this process very attractive.

The main components of such an autoresonant magnetic isotope separator are presented in Fig. 1: (i) a cylindrical vessel, (ii) a set of coils located around the outside of the chamber producing a uniform magnetic field along the axis of the cylindrical vacuum chamber, (iii) a suitable pair of conductors wounded as a double helix around the chamber or a set of permanent magnet to produce a tapered magnetic field with circular polarization as in free electron laser devices, (iv) an ion beam source at one end of the separator, and (v) collecting plates at the other end.

In this work, we identify and calculate analytically the tapered magnetic structure allowing an efficient mass-dependent conversion of linear to angular momentum. A Hamiltonian dynamic provides the right framework to identity and analyze ion autoresonance in our tapered magnetic device. We proceed as follows. First, we write down the Hamilton equation in which the helicity of the undulator $k(z)$ is kept as a free parameter. For one specific specie, we require a continuous conversion of linear to angular momentum; this constraint yields Eq. (3). Finally, we check that the other isotopes stay off resonance so that linear momentum conversion remains in the adiabatic regime.

The paper is organized as follows. In Sec. II, we present the model used to define the magnetic field produced by an ideal tapered undulator. In Sec. III, starting from the Hamiltonian of one ion in the tapered magnetic structure, we identify and determine the autoresonance conditions and then calculate and study the corresponding magnetic structure that permits a resonant interaction between the fields and the particles. In Sec. IV, we complete this study by a set of numerical simulations of ion orbits in the magnetic structure with realistic fields and length values. These simulations completely validate our analytical findings and the remarkable efficiency of this new process. Section V summarizes our results and gives our conclusions.

In order to simplify, we will consider single charged ions ($Z=1$), noting that the generalization to multiply charged ions is straightforward. In the following, except in the final discussion, we use the system of units $e=m_i=1$, where e is the electron charge and m_i the mass of the resonant ion.

II. MAGNETIC FIELD MODEL

Let us consider the following magnetic structure: a static homogeneous magnetic field $\mathbf{B}_o = \Omega \mathbf{e}_z$ plus a transverse circularly polarized static magnetic field $\mathbf{B}_\omega(z) = B_\omega[\cos(kz)\mathbf{e}_x + \sin(kz)\mathbf{e}_y]$. Ω is the amplitude of the uniform axial field component. Choosing a *Coulomb* gauge ($\nabla \cdot \mathbf{A} = 0$), these magnetic fields $\mathbf{B}_o$ and $\mathbf{B}_\omega$ derive, respectively, from the potential vectors $\mathbf{A}_o$ and $\mathbf{A}_\omega$, given by

$$\mathbf{A}_o = \Omega x \mathbf{e}_y \quad (4)$$

and

$$\mathbf{A}_\omega(z) = A\cos\varphi(z)\mathbf{e}_x + A\sin\varphi(z)\mathbf{e}_y. \quad (5)$$

We will refer to the axial or longitudinal direction as the direction along $\mathbf{e}_z$ and to the transverse direction to any direction in the plane $(\mathbf{e}_x, \mathbf{e}_y)$. In Eq. (5), the phase $\varphi(z)$ increases with z according to the following relation:

$$\varphi(z) = \int_0^z k(z)dz, \tag{6}$$

where $k(z)$ is the local helicity related to the undulator period λ through $k(z)=2\pi/\lambda(z)$. For a periodic undulator, k is constant and magnetic field lines follow perfect helicoidal trajectories. Here, since we anticipate a tapered undulator, we have introduced an unspecified function $k(z)$.

For this magnetic field model, the transverse rotating magnetic field is described by only two parameters, i.e., A and k, and its amplitude is $B_\omega = kA$. Note that these fields are divergence free ($\nabla \cdot \mathbf{B}=0$) but are not solenoidal ($\nabla \times \mathbf{B} \neq 0$). However, it can be easily shown ("near-axis approximation" in free electron laser studies[11–13]), by using a more realistic field, that the effect of the additional component providing a current-free condition can be safely neglected in front of the main component of this standard model. The undulator system outside the chamber will produce a transverse field with radial (r) inhomogeneities $A \sim I_1(kr)$, where I_1 is the modified Bessel function of first kind; this current-free vector potential reduces to (5) near the axis. Here, we make the assumption that the monoenergetic multi-isotope ion beam propagates close enough to the axis so that we can neglect the radial variation of this magnetic field. Note that such tapered helical undulators are currently used for free electron lasers and are usually modeled with this standard model; i.e., Eq. (5).

III. HAMILTONIAN

A. Resonant isotope dynamics

To compute the right shape of the helical tapered magnetic field [Eq. (3)], we consider first the resonant isotope dynamics. The particles enter the circularly polarized tapered magnetic field along the z axis at position $(0,0,0)$ with kinetic energy $E=\frac{1}{2}P_0^2$.

In normalized units, the time-independent classical Hamiltonian describing the interaction between an ion and a static magnetic field is given by

$$H(\mathbf{r},P) = \frac{1}{2}[\mathbf{P} - \mathbf{A}(\mathbf{r})]^2, \tag{7}$$

where $\mathbf{r}=(x,y,z)$ are the spatial coordinates, $\mathbf{P}=(P_x,P_y,P_z)$ is the canonical momentum conjugated to $\mathbf{r}$, and $\mathbf{A}=\mathbf{A}_0+\mathbf{A}_\omega$ is the potential vector. To separate the slow and the fast time scales of the motion, let us introduce the following generating function:[14]

$$F_3(\alpha,Y,Z,P_x,P_y,P_z) = -\frac{P_x P_y}{\Omega} - \frac{P_x^2}{2\Omega}\tan\alpha - YP_y - ZP_z, \tag{8}$$

in order to perform a canonical transformation. This transformation introduces the new set of canonical variables (α,Y,Z,J,P_Y,P) related to the old set by

$$x = \frac{P_Y}{\Omega} + \sqrt{\frac{2J}{\Omega}}\sin\alpha, \tag{9a}$$

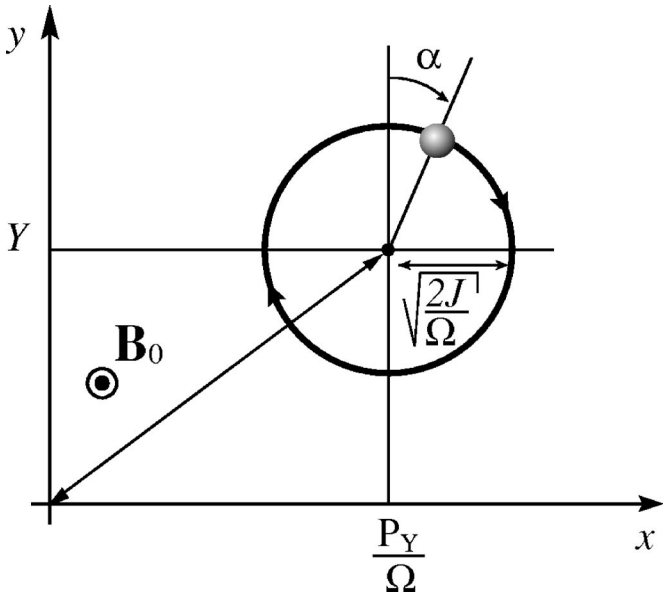

FIG. 2. Definitions of the "new" variables: P is the longitudinal momentum, $\sqrt{2\Omega J}$ the transverse momentum, α the gyro-angle, and Y and P_Y/Ω are the guiding center coordinates along, respectively, $\mathbf{e}_y$ and $\mathbf{e}_x$.

$$y = Y - \sqrt{\frac{2J}{\Omega}}\cos\alpha, \tag{9b}$$

$$z = Z, \tag{9c}$$

$$P_x = \sqrt{2\Omega J}\cos\alpha, \tag{9d}$$

$$P_y = P_Y, \quad P_z = P. \tag{9e}$$

These new variables have the following meanings (see Fig. 2): P is the longitudinal momentum, $\sqrt{2\Omega J}$ the transverse momentum, $\sqrt{2J/\Omega}$ the Larmor radius, α the gyro-angle (cyclotron phase), and Y and P_Y/Ω are the guiding center coordinates along, respectively, $\mathbf{e}_y$ and $\mathbf{e}_x$.

The Hamiltonian expressed with this set of variables is given by

$$H(\alpha,z,J,P) = \frac{1}{2}A^2 + \frac{1}{2}P^2 + \Omega J - A\sqrt{2\Omega J}\cos[\varphi(z)-\alpha]. \tag{10}$$

In this relation (10), the first term is proportional to the magnetic energy $B_\omega^2/2\mu_0$, the second and third ones to the ion kinetic energy, and the last one models the interaction between the ion and the field. We point out that the guiding center coordinate Y and the canonical momentum P_Y are cyclic variables (they do not appear in the Hamiltonian) and are, thus, constants of motion that can be set to zero without any loss of generality.

To identify and calculate the required magnetic tapered structure allowing for autoresonance, we now consider the Hamilton motion equation derived from the Hamiltonian (9)

$$\frac{d\alpha}{dt} = \frac{\partial H}{\partial J} = \Omega - \frac{A\Omega}{\sqrt{2\Omega J}}\cos[\varphi(z)-\alpha], \tag{11a}$$

$$\frac{dz}{dt} = \frac{\partial H}{\partial P} = P, \tag{11b}$$

$$\frac{dJ}{dt} = -\frac{\partial H}{\partial \alpha} = A\sqrt{2\Omega J}\,\sin[\varphi(z) - \alpha], \tag{11c}$$

$$\frac{dP}{dt} = -\frac{\partial H}{\partial z} = -A\sqrt{2\Omega J}k(z)\sin[\varphi(z) - \alpha]. \tag{11d}$$

The factor $\varphi(z)-\alpha$ is the relative phase between the gyroangle α and the field phase $\varphi(z)$.

At this stage of the analysis, the magnetic field phase $\varphi(z)$ is still unspecified. As we will see, a unique specification of the undulator parameter $k(z)$ will allow continuous energy transfer from longitudinal to transverse degree of freedom; i.e., *autoresonance*.

Now, consider Eqs. (11c) and (11d) describing, respectively, the rates of change of transverse and longitudinal momentum. Suppose we turn off the transverse magnetic field $A=0$; the actions J and P will then be constant and the gyroangle α will rotate uniformly in time. When the transverse component A is turned on ($A \neq 0$), the action J (P) will increase continuously (decrease continuously) if the phase $\varphi(z)-\alpha(t)$ remains constant and is equal to $\pi/2$. This phase-locking condition reads

$$\varphi(z) - \alpha(t) = \frac{\pi}{2}. \tag{12}$$

Inplementing this phase-locking condition (12) into Hamilton equations (11), we get the following equations of motion at the *autoresonance*:

$$\frac{d\alpha}{dt} = \frac{\partial H}{\partial J} = \Omega, \tag{13a}$$

$$\frac{dz}{dt} = \frac{\partial H}{\partial P} = P, \tag{13b}$$

$$\frac{dJ}{dt} = -\frac{\partial H}{\partial \alpha} = A\sqrt{2\Omega J}, \tag{13c}$$

$$\frac{dP}{dt} = -\frac{\partial H}{\partial z} = -A\sqrt{2\Omega J}k(z). \tag{13d}$$

Equations (13) complemented by the definition (6) define implicitly the variation of the periodic modulation $k(z)$ for which autoresonance occurs. In others words, we face an inverse problem in which a steady resonant interaction of a cyclotron kind between charged particles and an unknown fields is assumed. Integrating Eq. (13c) with the initial conditions $J(0)=0$ yields

$$\sqrt{2\Omega J} = A\Omega t, \tag{14}$$

describing linear increase of the transverse momentum with respect to time. This increase of the transverse momentum takes place at the expense of the longitudinal one. Then, differentiating with respect to time the phase-matching condition (12), we obtain a local relation between $k(z)$, the longitudinal momentum P, and the cyclotron frequency Ω:

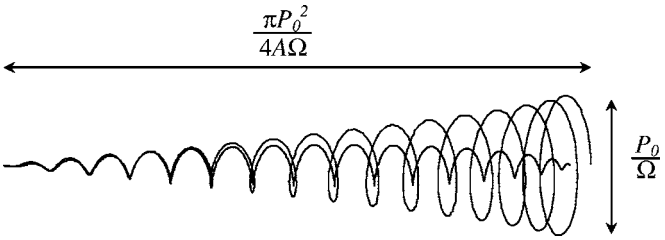

FIG. 3. Trajectory of a resonant ion for $A/P_o=10^{-2}$; $L=\pi P_0^2/4A\Omega$ is the distance traveled along $\mathbf{e}_z$ for which all the energy has been transferred to the transverse degree of freedom. The final radius is P_o/Ω.

$$\frac{d[\varphi(z) - \alpha]}{dt} = \frac{dz}{dt}\frac{d\varphi(z)}{dz} - \Omega = k(z)P - \Omega = 0 \tag{15}$$

since $k(z)=d\varphi(z)/dz$ [see Eq. (6)]. Introducing this *autoresonant condition* $kP=\Omega$ relation into Eq. (13d) and integrating with respect to time, we obtain the time dependence of the longitudinal canonical momentum P:

$$P(t) = P_0\sqrt{1 - \left(\frac{A\Omega t}{P_0}\right)^2}. \tag{16}$$

This equation shows that when the autoresonant condition is fulfilled, the energy transfer from the longitudinal to the transverse degree of freedom occurs at the time

$$\tau = \frac{P_o}{A\Omega}. \tag{17}$$

The final step is to integrate Eq. (13b), giving

$$z(t) = \frac{P_o^2}{2A\Omega}\left[\arcsin\frac{A\Omega t}{P_0} + \frac{A\Omega t}{P_0}\sqrt{1 - \left(\frac{A\Omega t}{P_0}\right)^2}\right]. \tag{18}$$

We can now find the full length L of the undulator as a function of the parameters A, P_o, and Ω:

$$L = z(\tau) = z\left(\frac{P_o}{A\Omega}\right) = \frac{\pi P_o^2}{4A\Omega}. \tag{19}$$

From Eqs. (9a), (9b), (14), and (18) we also obtain the parametric equations of the path followed by a resonant particle:

$$x(t) = At\,\sin\Omega t, \tag{20a}$$

$$y(t) = At\,\cos\Omega t, \tag{20b}$$

$$z(t) = \frac{P_o^2}{2A\Omega}\left[\arcsin\frac{A\Omega t}{P_0} + \frac{A\Omega t}{P_0}\sqrt{1 - \left(\frac{A\Omega t}{P_0}\right)^2}\right]. \tag{20c}$$

The resonant ion path follows a helix (see Fig. 3) whose radius increases linearly with respect to time.

To express the undulator period as a function of the distance z, we first relate longitudinal position z and helicity k through

$$\frac{2A\Omega}{P_o^2}z(k) = \left[\arcsin\sqrt{1-\left(\frac{\Omega}{kP_o}\right)^2} + \frac{\Omega}{kP_o}\sqrt{1-\left(\frac{\Omega}{kP_o}\right)^2}\right]. \quad (21)$$

Equation (21) constitutes the main results of this study and gives the variation of the pitch of the magnetic field line $\lambda = 2\pi/k$ as a function of the distance traveled along the main axis and of the three parameters P_o, Ω, and A. We note that this function depends on the resonant isotope mass through Ω and $P_o=(2E/m_i)^{-1/2}$. It turns out that, given the values of Ω, P_o, and A, the undulator parameters are fully determined. To study and invert this function, we introduce the two dimensionless variables K and Z, given by

$$K = \frac{kP_o}{\Omega}, \quad Z = \frac{2A\Omega}{P_o^2}z. \quad (22)$$

Equation (21) expressed with these dimensionless variables reads

$$Z = \arcsin\sqrt{1-\frac{1}{K^2}} + \frac{1}{K}\sqrt{1-\frac{1}{K^2}}. \quad (23)$$

To invert this function, we perform the change of variable $K \rightarrow \theta$ with $K=1/\cos\theta$, so that Eq. (23) becomes the celebrated *Kepler* equation

$$2Z = 2\theta + \sin 2\theta, \quad (24)$$

for the case where the eccentricity is equal to 1. The solution of the Kepler equation (24), i.e., $\theta(Z)$, can be written as a *Kapten* series of *Bessel* function of the first kind:[15]

$$\theta = Z + \sum_{n=1}^{+\infty}\frac{J_n(n)}{n}\sin 2n\left(Z-\frac{\pi}{2}\right), \quad (25)$$

which yields the following expression for the normalized helicity K:

$$K(Z) = \left\{\cos\left[Z + \sum_{n=1}^{+\infty}\frac{J_n(n)}{n}\sin 2n\left(Z-\frac{\pi}{2}\right)\right]\right\}^{-1}. \quad (26)$$

Finally, going back to the dimensional variables, i.e., the cyclotron frequency ω_c, the input velocity v_o, and the undulator potential A, we end up with the explicit formula (3) stated in Sec. I. Based on this original result giving the tapered helicity of the magnetic structure for isotope separation, we will perform a set of numerical simulations to check the efficiency of our device.

The normalized helicity function $K(Z)$ is plotted in Fig. 4. Full conversion occurs on a finite length $Z=\pi/2$, but requires that the helicity diverges (corresponding to an unphysical period equal to zero) at the end of the structure. The point $Z=\pi/2$ is an essential singularity and the function $K(Z)$ is nonanalytical at the exit. However, from (16), we remark that 87% (99%) of the linear to angular momentum conversion is achieved when $Z=1.48$ corresponding to $K=2$ ($Z=1.56$ corresponding to $K=4$). Hence, from a practical point of view, it is important to note that most of the linear to angular momentum conversion occurs for a twofold increase of the helicity (see Table I). The strong tapering at the very end of the structure appears to be useless for the purpose of isotope separation. This point is well summarized in Fig. 5, where we have plotted the ratio of the transverse energy ΩJ to the initial energy $P_o^2/2$ as a function of the normalized length Z.

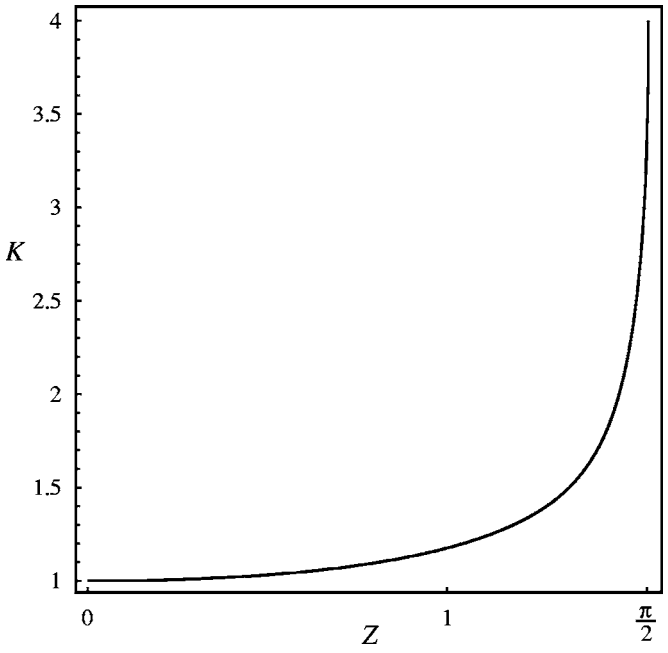

FIG. 4. Normalized undulator wave vector vs normalized length. Perpendicular to longitudinal momentum ratio vs normalized length.

To conclude this section, we derive the expression of the field phase $\varphi(Z)$, given by

$$\varphi(Z) = \int_0^{z(Z)} k(z)dz = \frac{P_o}{2A}\int_o^Z K(Z)dZ. \quad (27)$$

This last integral is evaluated by performing the change $K \rightarrow \theta$:

$$\varphi(Z) = \frac{P_o}{2A}\int_o^{\theta(Z)}\frac{1}{\cos\theta}\frac{dZ}{d\theta}d\theta = \frac{P_o}{A}\sin\theta, \quad (28)$$

and by invoking an identity relating the sinus of the eccentric anomaly θ to Z through[15]

$$\sin\theta = \sqrt{\frac{1}{4} + \sum_{n=1}^{+\infty}\frac{J_n'(n)}{n}\cos 2n\left(Z-\frac{\pi}{2}\right)}. \quad (29)$$

At the end of the undulator $Z=\pi/2$, $\theta=\pi/2$; hence, $\varphi = P_o/A$ and the total number of rotations N undergoes by a magnetic field line is thus $P_o/(2\pi A)$.

TABLE I. Energy transfer versus traveled length in the undulator.

K	1	2	3	4	5
Z	0	1.48	1.55	1.56	1.565
$(2\Omega J)^{1/2}/P_o(\%)$	0	87	94	97	99

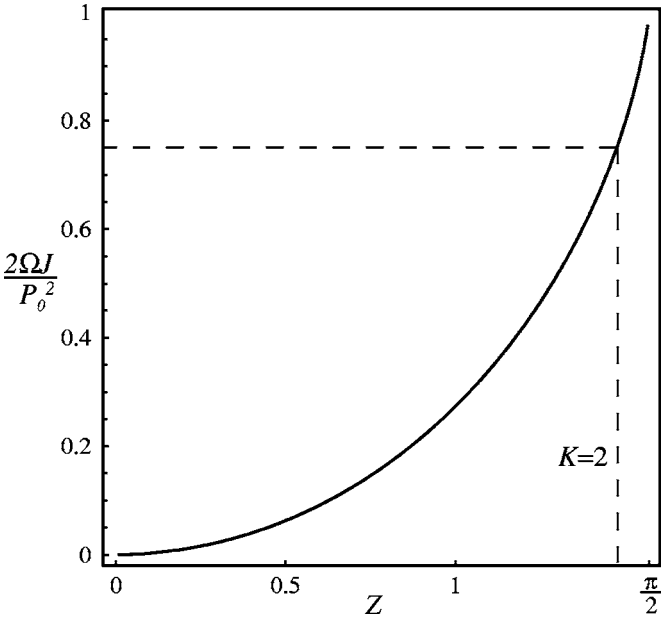

FIG. 5. Perpendicular to longitudinal momentum ratio vs normalized length.

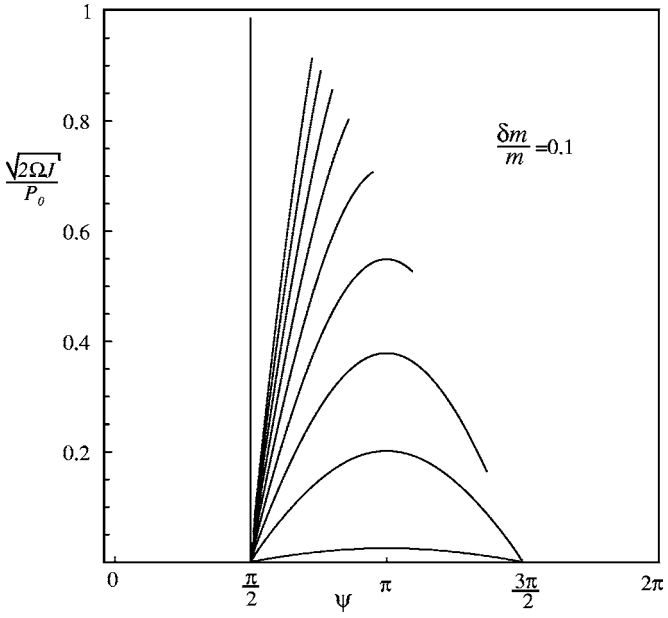

FIG. 6. Phase portrait in the (ψ,J) plane for various value of A/P_0. The straight line corresponds to the resonant ion for which the phase-locking condition Eq. (12) holds.

B. Nonresonant isotope dynamics

Let us now consider the nonresonant ion dynamics. The undulator helicity equation (3) depends on a specific isotope mass through P_o and Ω.

To derive a separation criterion, we study with a perturbation techniques the nonresonant isotope dynamic. Let δm be the difference between the resonant isotope mass m_i and the nonresonant isotope mass. The resonant condition (15) depends on the resonant isotope mass through initial linear momentum $P_o(m_i)=(2E_c/m_i)^{1/2}$ and cyclotron frequency $\Omega(m_i)=eB_o/m_i$. For the nonresonant isotope, the resonance mismatch is to the first order in the parameter $\delta m/m_i$:

$$kP(m_i+\delta m)-\Omega(m_i+\delta m)\sim\frac{\delta m}{2m_i}\Omega. \tag{30}$$

Let $\psi=\varphi-\alpha$ be the difference between the field phase and the gyro-angle. Using ψ rather than α as a dynamical variable, we rewrite the set of motion equations (11) as

$$\frac{d\psi}{dt}=kP-\Omega-\frac{A\Omega}{\sqrt{2\Omega J}}\cos\psi, \tag{31a}$$

$$\frac{dz}{dt}=P, \tag{31b}$$

$$\frac{dJ}{dt}=A\sqrt{2\Omega J}\sin\psi, \tag{31c}$$

$$\frac{dP}{dt}=-A\sqrt{2\Omega J}k(z)\sin\psi. \tag{31d}$$

In the *resonant* case, $kP-\Omega=0$ and ψ is a constant equal to $\pi/2$ [see Eq. (12)]. In the *nonresonant* case $kP-\Omega\sim-\delta m/2m_i\Omega$ and the phase ψ is no longer a constant of the motion; the sine function in Eqs. (31c) and (31d) are now oscillating. Figure 6 displays these different ion dynamics in the (ψ,J) plane. The straight line corresponds to the phase-locking condition $\psi=\varphi-\alpha=\pi/2$ and the others paths to nonresonant dynamics. Substituting Eq. (30) into Eq. (31a) and integrating (31a) and (31c), we obtain

$$\psi=\frac{\pi}{2}-\frac{\delta m}{4m}\Omega t,$$

$$\sqrt{2\Omega J}=\frac{A}{\frac{\delta m}{4m}}\sin\frac{\delta m}{4m}\Omega t.$$

In the nonresonant case, we see that the transverse momentum $\sqrt{2\Omega J}$ is now an oscillating function with a period equal to $\tau_{nr}=8\pi m/\delta m\Omega^{-1}$. Note that in the limit $\delta m/m=0$, we recover as expected the resonant result (14).

The separation process is *efficient* when the period τ_{nr} is much smaller than the resonant energy transfer time τ [given by Eq. (17)]. When this criterion is fulfilled, the energy transfer from longitudinal to transverse degree of freedom for the nonresonant isotope is, as required, small. From $\tau_{nr}\ll\tau$, results the following separation criterion:

$$\frac{P_o}{8\pi A}\gg\frac{m}{\delta m}. \tag{32}$$

Since the number of magnetic field line rotations N is $P_o/(2\pi A)$, this criterion can also be written

$$N\gg\frac{m}{4\delta m}. \tag{33}$$

For a given relative mass difference $\delta m/m$, ion initial linear momentum P_0 and the rotating magnetic field parameter A each have to be set to a certain value in order to satisfy this separation criterion.

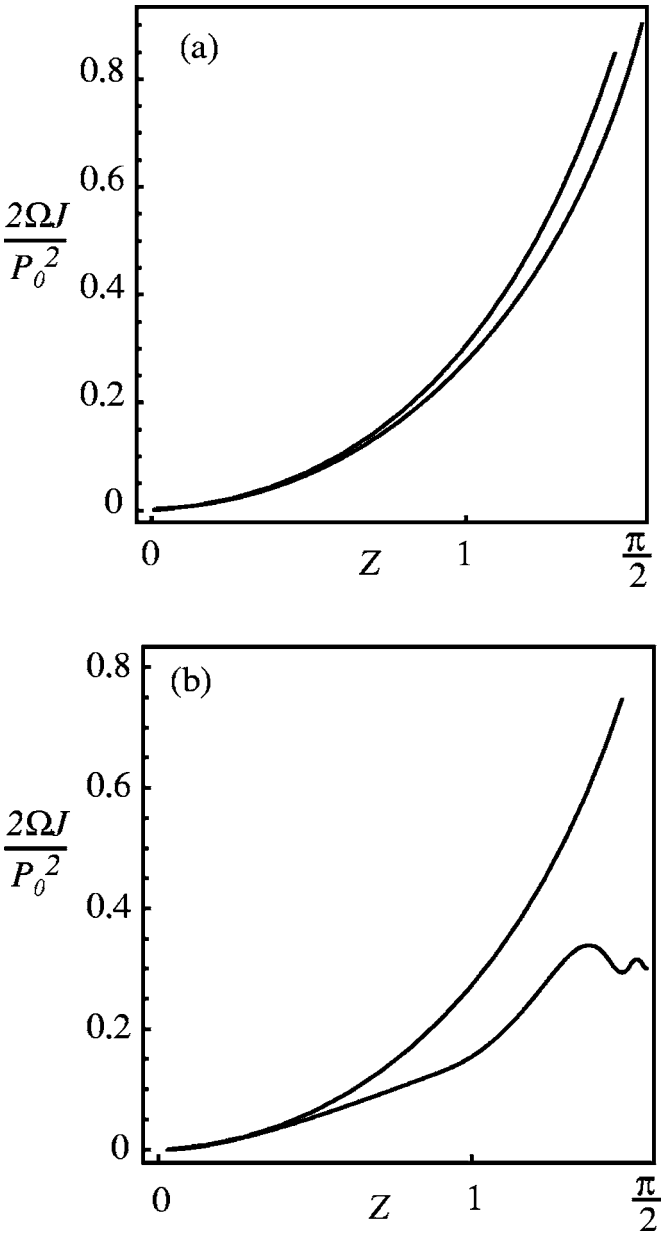

FIG. 7. Ratio of the perpendicular energy to the initial energy vs length. The relative mass ration is equal to 10% (neon case). (a) For $A/P_o=10^{-1}$, the separation criterion is not fulfilled and both isotope follow the same trajectory. (b) For $A/P_o=10^{-2}$ the separation criterion is satisfied.

IV. NUMERICAL VALIDATION

To validate our study, we have performed a numerical simulation to solve Newton's equations for two isotopes. As a test case, let us take neon and the two ions $^{20}Ne^{+}$ and $^{22}Ne^{+}$, and the corresponding relative mass ratio $\delta m/m$ is 0.1. Hence, from Eq. (32), to separate Ne^{20} and Ne^{22}, A/P_o must be set to a smaller value than 10^{-2}. To validate this separation criterion, we integrated Newton's equation for $A/P_o=10^{-1}$ and $A/P_o=10^{-2}$. The results are shown in Fig. 7. Clearly, when the separation criterion is fulfilled [see Fig. 7(b)], we observe isotope separation. Otherwise, if the separation criterion is not satisfied [see Fig. 7(a)], the resonance mismatch of the nonresonant species is so weak that linear to momentum conversion occurs for the two isotopes. Consequently, the two species are not separated.

V. DISCUSSION

It may be useful to point out that the method of resonance employed here enjoys certain similarities to resonant mechanisms that occur in the context of other plasma processes and other plasma applications. The use of guide fields together with helical fields is a method for free electron laser interaction, where the electron energy is extracted for the purpose of radiation generation, and this method has been considered in mathematical detail (see, e.g., Refs. 16–18). The use of static perturbations superposed upon a large axial field has also been adduced as a mechanism that may keep electrons from running away in an applied axial electric field in a tokamak.[19] In both of these instances, the slowing down occurs by means of resonant interaction with a static magnetic ripple field, which selects electrons with a specific parallel velocity. In the case of the free electron laser, the energy of the oscillating electron can be radiated into an electromagnetic mode. In the case of the runaway electrons in a tokamak, the maximum runaway energy may be clamped by the resonance. The release of resonant particle energy to a wave can also occur in a diffusive process, if the diffusion in energy is coupled to diffusion in space, such that a population inversion occurs in the joint velocity-configuration space.[20] In this respect, the tapered undulator performs a similar function in that the change in parallel energy is accompanied by an increase in radial position through the increase in Larmor radius.

VI. CONCLUSION

We have discovered and analyzed a class of tapered undulator able to perform full mass-dependent phase-matched conversion from linear momentum to angular momentum. The position-dependent helicity of this class of undulator depends on two parameters k_0 and ζ and is given by the following expression:

$$k(z)=\frac{k_0}{\cos\left[\frac{z}{\zeta}+\sum_{n=1}^{+\infty}\frac{J_n(n)}{n}\sin 2n\left(\frac{z}{\zeta}-\frac{\pi}{2}\right)\right]}. \tag{34}$$

A given undulator corresponds to specific values of k_0 and ζ, and a resonant interaction between the magnetic field and an ion occurs if the following relations are fulfilled:

$$\frac{\omega_c}{v_o}=k_0, \tag{35a}$$

$$\frac{p_o}{2eA}\frac{v_o}{\omega_c}=\zeta. \tag{35b}$$

Moreover, isotope separation occurs if $p_0/eA \gg 8\pi m/\delta m$ [see Eq. (32)], i.e., from (35), if the following condition is fulfilled:

$$k_0\zeta \gg 4\pi\frac{m}{\delta m}. \tag{36}$$

$R=k_0\zeta$ is the mass resolution of the devices. For convenience, rather than k_0 and ζ, we will use in the following analysis R and k_0 for the device parameters. Expressed with R and k_0, the resonance condition (35a) and the isotope separation conditions (35b) can be rewritten

$$\frac{\omega_c}{v_o} = k_0, \tag{37a}$$

$$\frac{p_o}{2eA} = R. \tag{37b}$$

Noting the following scaling $\omega_c/v_o \sim B_0/E^{1/2}m_i^{1/2}$ and $p_o/eA \sim m^{1/2}E^{1/2}/A$, we remark that the conditions (37) for resonance requires in fact to set only one value among the parameters A, E, or B_0. The values of the two others parameters being imposed by the two conditions (37).

Let us consider the following example of an undulator with mass resolution $R=100$ and helicity at the entrance k_0 equal to 10 m^{-1}. These last characteristics correspond to the following condition (A is the atomic mass and Z is the ion charge):

$$k_0 = 217\frac{Z}{A^{1/2}}\left(\frac{[1\ \mathrm{keV}]}{E}\right)^{1/2}\left(\frac{B}{[1\ \mathrm{T}]}\right) = 10\ \mathrm{m}^{-1}. \tag{38}$$

For neon, for example, $A\sim 20$, this value can be obtained for typical values $E\sim 25$ keV and $B\sim 1$ T. With these parameters, the full length of the device is

$$L = \frac{\pi}{2}\zeta = \frac{\pi}{2}\frac{R}{k_0} \sim 15\ \mathrm{m}. \tag{39}$$

It must be pointed out that this length can be reduced by using multiply charged ions. Indeed, going back to SI variables, we see from (18), that this length scales as Z^{-2}. However, the final radius v_o/ω_c scales as Z^{-1}.

[1] M. W. Grossman and T. A. Shepp, IEEE Trans. Plasma Sci. **19**, 1114 (1991).
[2] J. M. Dawson, H. C. Kim, D. Arnush *et al.*, Phys. Rev. Lett. **37**, 1547 (1976).
[3] T. Mieno, Nucl. Instrum. Methods Phys. Res. B **70**, 33 (1992).
[4] T. Mieno, Nucl. Instrum. Methods Phys. Res. B **70**, 37 (1992).
[5] T. Ikehata, Nucl. Instrum. Methods Phys. Res. B **70**, 26 (1992).
[6] I. A. Kotelnikov and S. G. Kuzmin, Plasma Phys. Rep. **25**, 1095 (1999).
[7] V. I. Volosov, I. A. Kotelnikov, and S. G. Kuzmin, Plasma Phys. Rep. **24**, 474 (1998).
[8] A. I. Karchevskii and E. P. Potanin, Plasma Phys. Rep. **20**, 214 (1994).
[9] R. Hatakeyama and N. Sato and N. Sato, Nucl. Instrum. Methods Phys. Res. B **70**, 21 (1992).
[10] A. Compant La Fontaine and V. G. Pashkovsky, Phys. Plasmas **2**, 4641 (2006).
[11] C. W. Robertson and P. Sprangle, Phys. Fluids B **1**, 3 (1989).
[12] P. Diament, Phys. Rev. A **23**, 2537 (1981).
[13] J. Fajans, D. A. Kirkpatrick and G. Bekefi, Phys. Rev. A **32**, 3448 (1985).
[14] H. Goldstein, *Classical Mechanics* (Addison-Wesley, Reading, MA, 1950), Chap. VIII, pp. 237–247.
[15] G. N. Watson, *A Treatise on the Theory of Bessel Functions* (Cambridge University Press, Cambridge, 1966), Chap. XVII, pp. 553–555.
[16] I. B. Bernstein and L. Friedland, Phys. Rev. A **23**, 816 (1981).
[17] L. Friedland and A. Fruchtman, Phys. Rev. A **25**, 2693 (1982).
[18] A. Fruchtman and L. Friedland, IEEE J. Quantum Electron. **19**, 327 (1983).
[19] L. Laurent and J. M. Rax, Europhys. Lett. **11**, 219 (1990).
[20] N. J. Fisch and J. M. Rax, Phys. Rev. Lett. **69**, 612 (1992).